

Investigating shear band interaction in metallic glasses by adjacent nanoindentation



Hu Huang, Jiwang Yan*

Department of Mechanical Engineering, Faculty of Science and Technology, Keio University, Yokohama 223-8522, Japan

ARTICLE INFO

Keywords:

Metallic glass
Shear band
Interaction
Nanoindentation
Reactivation
Serrated flow

ABSTRACT

The plastic deformation of metallic glass (MG) at room temperature progresses mainly through shear banding. Although many previous studies have addressed the behaviors of the shear band (SB), there is still some debate regarding the SB processes, particularly its reactivation and interaction. Hence, it is essential to further understand the SB processes in MGs. In this paper, a new method via adjacent nanoindentation was introduced to investigate the SB interaction, which makes it easy to distinguish between the pre-existing and newly generated SBs. Nanoindentation was performed on Zr-based MG under various spatial intervals, and the resultant residual morphologies and serrated flows were comparatively analyzed. With a change in the interval, various SB behaviors, such as straight SBs, SB reactivation, stoppage, intersection, narrowing, and suppression were clearly observed in the interaction region. The evolution of the SBs indicated that the main carrier of the plastic deformation in the interaction region changed between the newly generated SBs and the pre-existing SBs. Corresponding to the strong SB interaction, serrated flows in the load-depth (P - h) curves were also found to be promoted. These findings are expected to enhance our understanding of SB processes, which is meaningful for controlling the SBs and tuning the surface plasticity of MGs.

1. Introduction

Although metallic glasses (MGs) possess unique mechanical, physical and chemical properties such as high strength and hardness, as well as excellent resistance to wear and corrosion, the application of MGs as structural and functional materials is considerably hindered because of their very limited ductility at room temperature [1,2]. As the plastic deformation of MGs at room temperature progresses mainly through shear banding [3,4], understanding the initiation, propagation, stoppage, and intersection of the shear band (SB) is important for controlling the plastic deformation of MGs and improving their ductility.

When uniaxial tension is applied at room temperature, a single SB and/or a few main SBs quickly propagate through the whole sample, resulting in the catastrophic failure of the MGs. If the propagation of individual SBs could be effectively hindered while multiple SBs are triggered, the plasticity of the MGs could be improved. Accordingly, many studies have attempted to tune the plasticity of MGs by controlling the SB processes [5–11]. For example, by introducing second-phase crystalline particles, SB propagation can be blocked and/or SB branching can be triggered, forming multiple SBs, and thus, the plasticity of MGs is improved [8,9]. By introducing pre-existing SBs via the

pre-deformation of MGs through processes such as cold rolling and surface shot-peening, the plasticity of MGs can also be changed by the reactivation of those pre-existing SBs and the extensive interaction with the newly generated SBs [5,6]. However, there remains some debate regarding this method as both work softening and work hardening have been reported [3,4]. This debate hinges on the direction of the pre-existing SBs with respect to the subsequent loading direction [6]. If the direction of the pre-existing SBs is parallel or close to the direction of the maximum shear stress in subsequent loading, those pre-existing SBs could be easily reactivated because they are weak regions with excess free volume, which propagate quickly, resulting in significant softening. Otherwise, however, new SBs could be induced by the subsequent loading but their propagation could be blocked by those pre-existing SBs. Thus, multiple SBs could be induced and they intersect with those pre-existing SBs. The frequent intersection of SBs could inhibit the plastic flow in MGs and thus result in work hardening. Hence, the pre-existing SB direction and pre-deformation process should be optimized.

Similarly, there remains some debate regarding pre-existing SBs inducing softening and hardening [12–15]. It has been experimentally confirmed that a single SB induces a softened region with decreased nanoindentation hardness compared with that of the surrounding matrix [16]. Thus, pre-existing SBs have been used to explain the decrease

* Corresponding author.

E-mail addresses: huanghuzy@163.com (H. Huang), yan@mech.keio.ac.jp (J. Yan).

<http://dx.doi.org/10.1016/j.msea.2017.08.040>

Received 20 June 2017; Accepted 10 August 2017

Available online 12 August 2017

0921-5093/ © 2017 Elsevier B.V. All rights reserved.

in the hardness of pre-deformed MGs. However, it has also been reported that pre-existing SBs can result in an increase in the hardness of pre-deformed MGs by promoting the intersection of SBs [14].

From the abovementioned analysis, we can note that the debate focuses on the SB processes, especially the reactivation and interaction. Hence, further investigation of the SB processes in MGs is urgently required. Previous studies have made great efforts to clarify the SB initiation and propagation [17–20], while SB reactivation and interaction have rarely been investigated, especially by experiment. Although SB reactivation and interaction have been widely used to explain deformation-induced softening and/or hardening in MGs [6,7,14,21,22], direct experimental evidence for the reactivation of SBs is insufficient and also their interaction with newly generated SBs is unclear. This is due to the technical difficulty associated with the observation of SB reactivation and interaction because it is difficult to distinguish individual SBs in time-scale by conventional experimental methods, especially when pre-existing SBs exist. Recently, Wang et al. [23] used scissors to cut a $\text{Cu}_{50}\text{Zr}_{50}$ MG ribbon and thus form multiple SBs with various interactions. By atomic force microscope (AFM) observation and analysis, they studied the mutual interaction between two SBs. However, this method is difficult to distinguish between SBs in time-scale because of the formation of relatively complex SB patterns. Thus, it cannot be applied to the study of the reactivation of pre-existing SBs and their interaction with newly generated SBs.

In this paper, we introduce adjacent nanoindentation as a new method for investigating the reactivation, deflection, stoppage, and intersection of SBs. By controlling the spatial interval, the SB interaction region could be created between adjacent indents. As the SBs for individual indents are arc-shaped, it is easy to distinguish between the SBs in time-scale by analyzing the SB direction. Thus, various SB behaviors could be observed and analyzed. These results are expected to enhance the understanding of SB processes, which is meaningful for controlling the SBs and tuning the plasticity of MGs.

2. Materials and experiments

2.1. Materials

The commonly used Zr-based MG, $\text{Zr}_{41.2}\text{Ti}_{13.8}\text{Cu}_{12.5}\text{Ni}_{10}\text{Be}_{22.5}$ (also called Vitreloy 1), was used in this study. One sample, with a diameter of 10 mm and a thickness of 1 mm, was cut from an as-cast MG rod by wire electrical discharge machining (wire-EDM). Because EDM results in the formation of crystallization layers [24,25], mechanical grinding using 400, 800, and 1500 grit sand papers, in sequence, was implemented first, after which the sample was polished to obtain a mirror surface for nanoindentation tests using 3.0, 1.0, 0.3 and 0.1 μm Al_2O_3 polishing suspensions, in sequence.

2.2. Adjacent nanoindentation

It is well known that nanoindentation using a Berkovich indenter induces the formation of arc-shaped SBs around the edges of a residual indent, as illustrated in Fig. 1 [26]. If another nanoindentation test is performed at a specific distance from the preceding one, an SB interaction region will be created between these two indents. Because of the arc-shape, it is easy to distinguish the SBs in time-scale by analyzing the direction of the arc, i.e., whether the SBs are formed as a result of the preceding or a subsequent nanoindentation. The SBs formed by preceding nanoindentation can be regarded as pre-existing SBs, and thus, the SB reactivation and interaction could be investigated by analyzing the SB characteristics in the interaction region. On the other hand, after the indenter is unloaded from the sample surface, compressive residual stress regions are generated around the edges, as shown in Fig. 1. Previous studies indicated that residual stress also affects the formation of SBs and further affects the plastic deformation of MGs [21,27,28]. Hence, by performing adjacent nanoindentation, the effects of residual

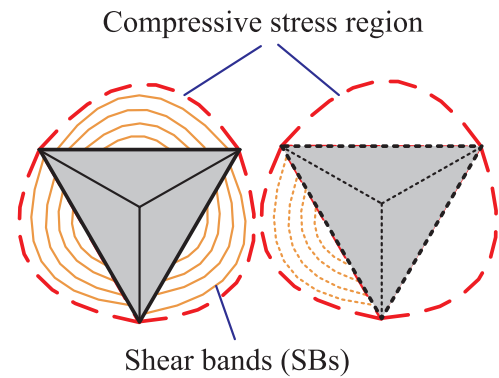


Fig. 1. Schematic of adjacent nanoindentation method.

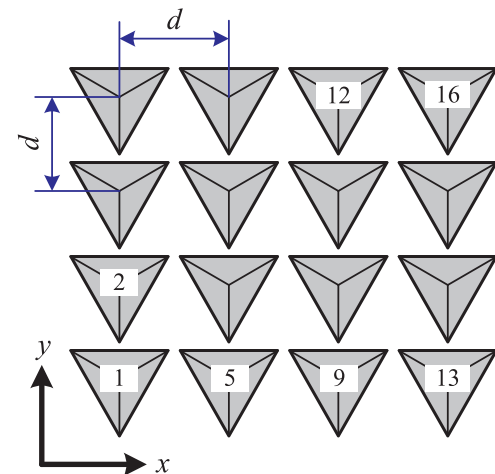


Fig. 2. Schematic showing 4×4 nanoindentation array with a spatial interval d between two adjacent indents.

stress on the SB behaviors could also be studied.

According to the adjacent nanoindentation method, 4×4 nanoindentation arrays like those illustrated in Fig. 2 were formed on the MG surface by using a commercial nanoindentation instrument (ENT-1100, Elionix Inc., Japan) equipped with a Berkovich-type diamond indenter. To facilitate the observation of the SBs, a relatively high indentation load of 1000 mN was used for all the nanoindentation tests to introduce easily observable SBs and SB interaction regions. To select a suitable spatial interval and loading rate, some nanoindentation tests were performed with an indentation load of 1000 mN and loading rates of 100 and 5 mN/s, prior to the adjacent nanoindentation experiments. The results indicated that the lengths of the edges of the residual indent were approximately 20 μm , and thus spatial intervals d of 15, 18, 20, 50, and 80 μm , were selected for comparison. Furthermore, the loading rates of 100 and 5 mN/s did not induce remarkable difference in the SBs, which could result from the high indentation load used here, given that the latter overwhelmed the effects of the loading rate on SBs. Therefore, to reduce the experimental time, a relatively high loading rate of 100 mN/s was selected for most of the nanoindentation tests. To correlate the SB interaction with the discontinuous depth change (commonly referred to as a “serrated flow” in the field of MGs) in the loading portion of the load-depth (P - h) curve, one 4×4 nanoindentation array was formed with an interval d of 20 μm under a loading rate of 5 mN/s.

2.3. Characterization

After nanoindentation, the three dimensional (3D) topographies of the indented regions were measured by using a Talysurf CCI1000 white

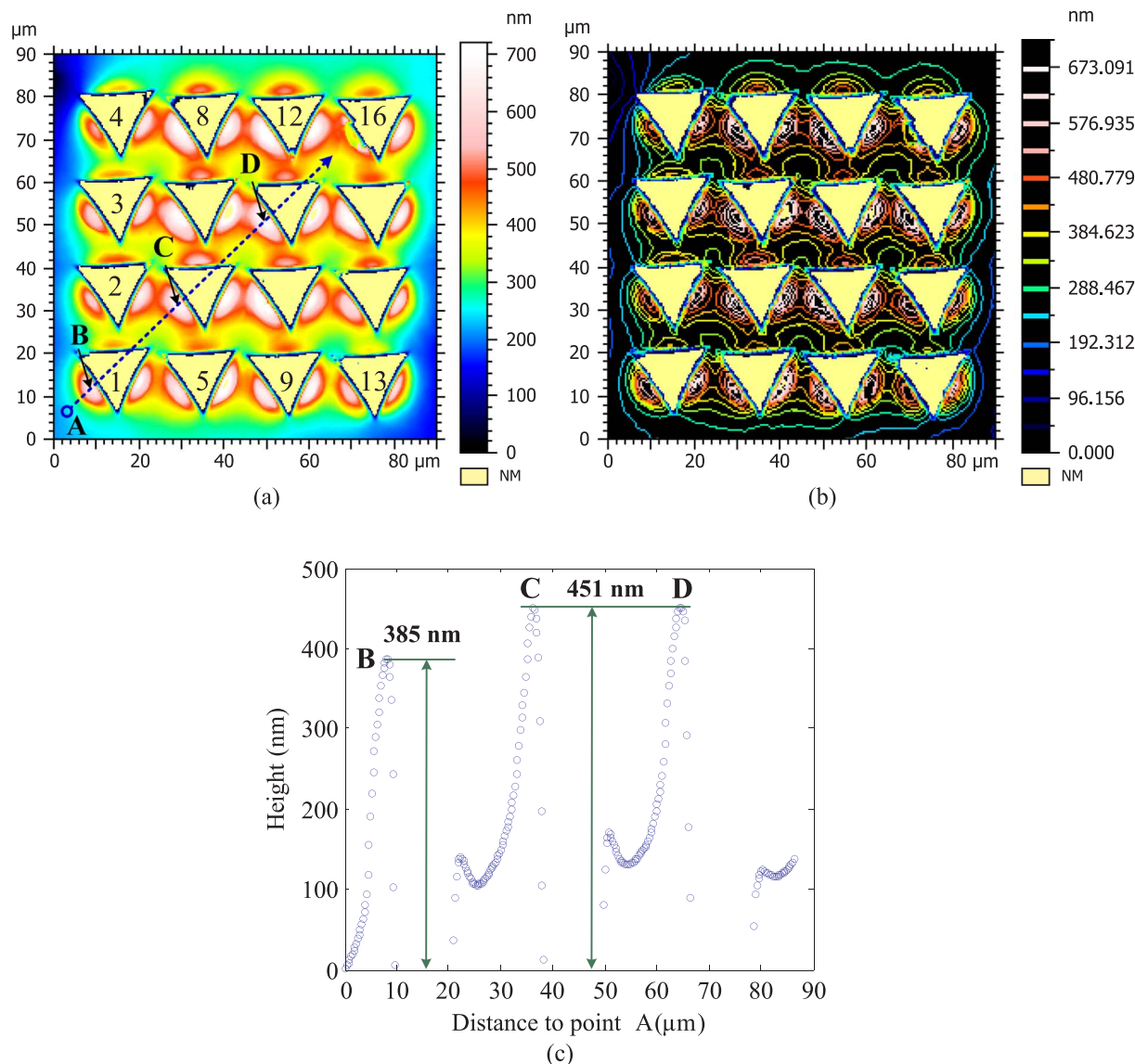


Fig. 3. (a) 3D topography and (b) contour of indentation region corresponding to interval d of 20 μm . (c) Profile of dotted line in (a).

light interferometer (AMETEK Taylor Hobson Ltd., UK). An atomic force microscope (AFM) (AFM 5100N, Hitachi, Japan) was used to characterize the local features of the interaction region between two adjacent indents. Furthermore, the indented regions were observed by using an environmental scanning electron microscope (ESEM) (Inspect S50, FEI, USA) and a field emission scanning electron microscope (FESEM) (JSM-7600F, JEOL, Japan) for higher magnification.

3. Results and discussion

3.1. Shear band characteristics

Fig. 3(a) and (b) show the 3D topography and contour, respectively, of the indentation region corresponding to an interval d of 20 μm . In Fig. 3(a), the height of the materials around the edges of each indent is considerable greater than that of the initial surface because of the extrusion of the MG materials during the interaction between the indenter and the sample surface. This phenomenon is commonly called “pile-up”. It is observed that preceding indents promote the formation of pile-ups during the subsequent nanoindentation tests, with higher and wider pile-ups being induced as shown, around indents 6, 7, 10, and 11. This is further confirmed by the profile indicated by the dotted line shown in

Fig. 3(a), as illustrated in Fig. 3(c). For No. 1 indent, the height of the pile-up is approximately 385 nm, while the height is approximately 451 nm for Nos. 6 and 11 indents. Furthermore, most of the pile-ups connect with adjacent pile-ups, as in the case between Nos. 6 and 10 indents and between Nos. 7 and 11 indents, which can be clearly seen from the contour of the indents shown in Fig. 3(b). The results shown in Fig. 3 indicate that strong interaction regions have formed between these indents as a result of the adjacent nanoindentation with an interval d of 20 μm .

Fig. 4(a) and (b) present the 3D topography and contour of the indentation region corresponding to an interval d of 50 μm . Although the middle region of these indents has been slightly elevated, the affected region for each indent can be easily distinguished, while the pile-ups have not connected with each other. In Fig. 4(b), the size of the indentation-affected region is roughly evaluated by using a circle to surround the indent. As a result, it is found to be about 24 μm . Because of the height segmentation shown in the scale bar, the actual size of the indentation-affected region should be slightly larger than 24 μm . It is for the reason that strong interaction regions are formed with an interval d of 20 μm in Fig. 3. However, for intervals of 50 and 80 μm , the interaction between the two adjacent nanoindentation tests is remarkably weakened.

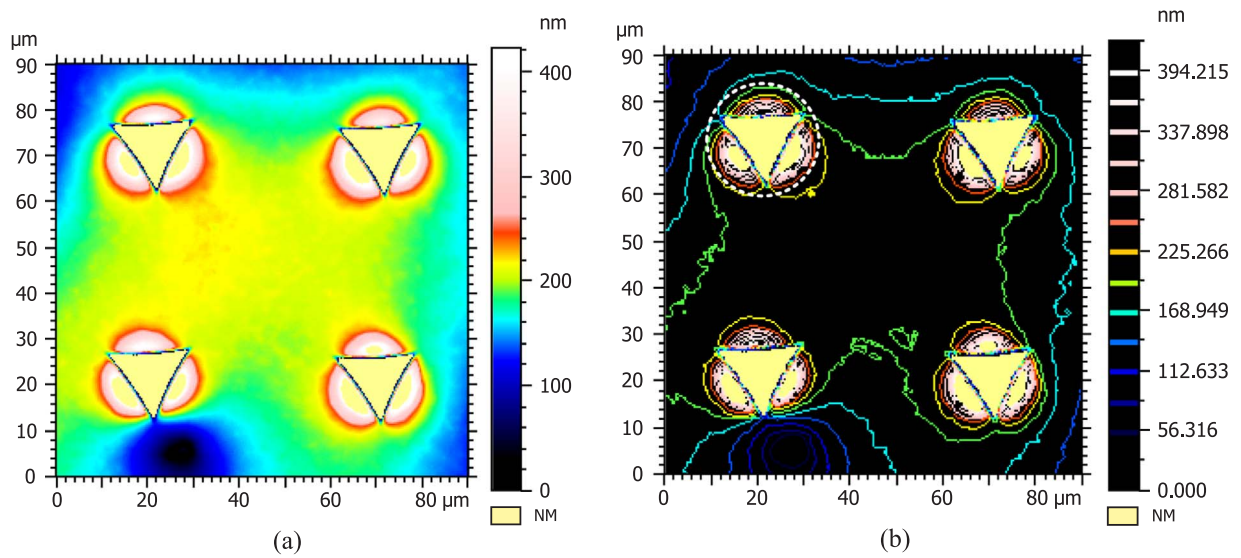


Fig. 4. (a) 3D topography and (b) contour of indentation region corresponding to interval d of 50 μm .

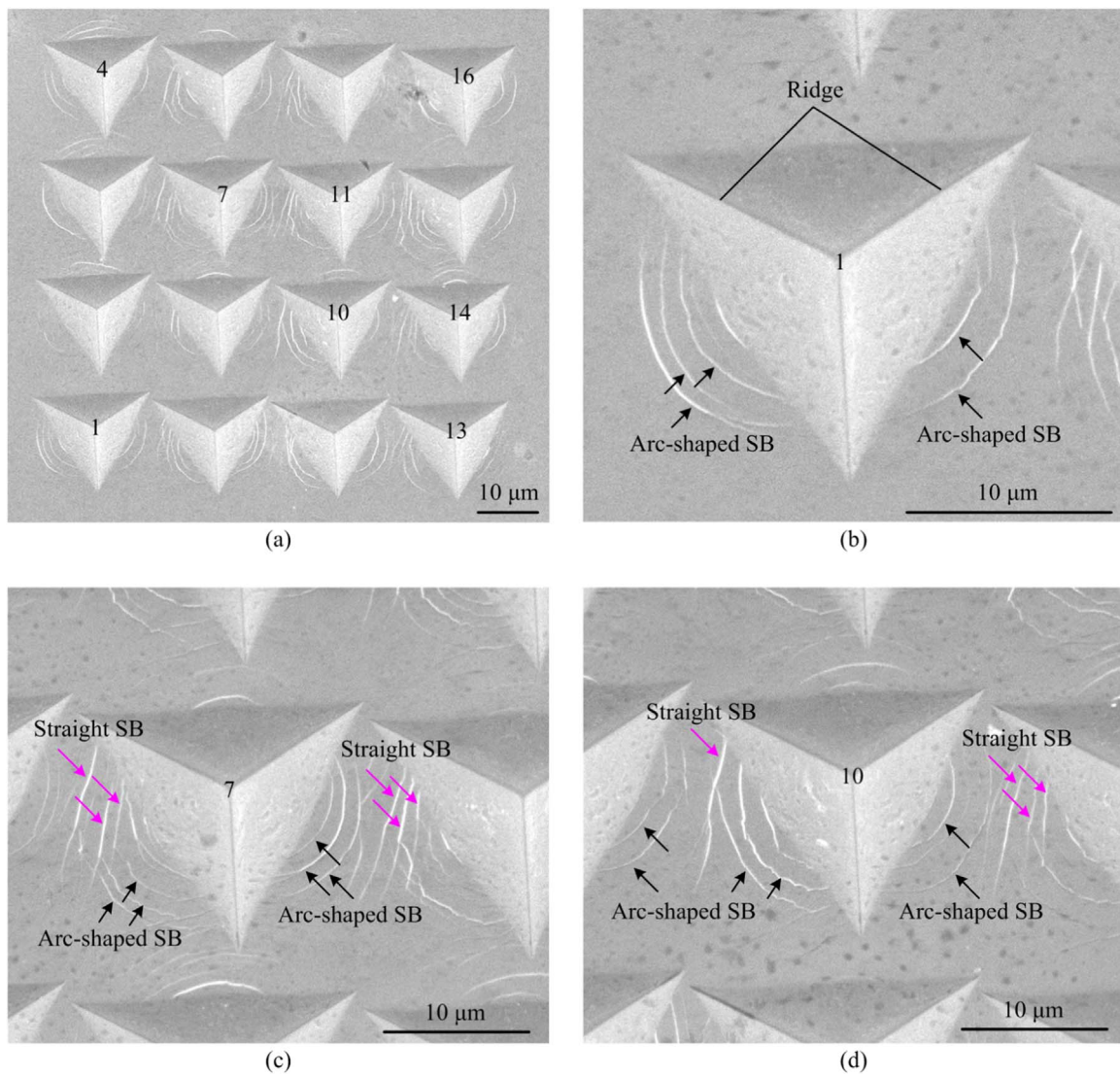


Fig. 5. (a) SEM morphology of indentation region corresponding to interval d of 20 μm . (b)–(d) show the enlarged morphologies corresponding to Nos. 1, 7, and 10 indents, respectively.

To analyze the detailed features of the interaction regions, Fig. 5(a) shows the SEM morphology of the indentation region corresponding to an interval d of 20 μm . Compared with the SBs to the left and right of the indents, it is commonly observed that less SBs are generated on the top of indents which results from the non-ideally perpendicular penetration of the indenter into the sample surface [29]. Note that in the interaction regions between two adjacent indents, not only are the pile-ups promoted as shown in Fig. 3 but also the SBs are intensively induced. For the nanoindentation of MGs without a pre-existing indent (No. 1 here), the SBs around the edges of the indent are arc-shaped, these being approximately symmetrical with respect to the corresponding ridge, as shown in Fig. 5(b). However, some straight SBs are observed to the left of Nos. 7, 8, 10–15 indents. Fig. 5(c) and (d) show the enlarged morphologies corresponding to Nos. 7 and 10 indents, respectively. Note that the SBs to the right of the indents in these two figures still exhibit a symmetrical arc-shape, while the symmetry has been perturbed on the left side, and some straight SBs can be clearly seen. The SBs to the left consist of two types, namely, straight SBs and arc-shaped SBs, and the interaction between these two types of SBs is observed. According to the nanoindentation testing sequence shown in Figs. 2 and 5(a), the results shown in Fig. 5(c) and (d) indicate that SB interaction regions have been successfully created with an interval d of 20 μm , while the preceding indents with SBs significantly affect the SB behaviors during subsequent nanoindentation tests.

Fig. 6(a) and (b) show representative SEM morphologies of the indents corresponding to intervals d of 50 and 80 μm , respectively. With an increase in the interval, the SBs around the indents gradually recover their symmetrical arc-shape, indicating that the interaction between two adjacent indents becomes weaker and weaker.

The results and discussion mentioned above are for intervals d greater than 20 μm . To further investigate the SB interaction, the following presents and discusses those cases with intervals d of 18 and 15 μm . Fig. 7 shows some representative SEM morphologies of the indents corresponding to an interval d of 18 μm . In Fig. 7(a) and its enlarged view, shown in Fig. 7(b), the SBs to the left of the indent exhibit strong asymmetry while they are still arc-shape with good symmetry on the right side. Furthermore, it is interesting to note that some SBs stop and connect with SBs with directions opposite to those of the arcs. According to the direction of the arc, the stopped SBs are newly generated while the SBs with the opposite directions belong to the preceding indent. This indicates that some SBs, formed by the preceding indent, are reactivated during the adjacent nanoindentation test. The

enhanced contrast at these SBs further confirms their reactivation. As shown in Fig. 7(b), the SB space between the non-reactivated and reactivated SBs (pre-existing SBs) decreases from the bottom to the top when SB stoppage and reactivation occur, implying that SB deflection also occurs together with the reactivation during the adjacent nanoindentation test to accommodate the plastic deformation.

In Fig. 7(c), SBs of the opposite direction appear and SB intersection where a newly generated SB passes through the pre-existing SBs is observed in Fig. 7(d). Compared with the change in the SB space shown in Fig. 7(b), in which SB stoppage and reactivation occur, the pre-existing SB space in Fig. 7(d) in which SB intersection occurs does not exhibit obvious decrease. Furthermore, the SB space of newly generated SBs sometimes narrows when SB intersection occurs, as shown in Fig. 7(e). Fig. 7(f) shows the SBs on the indent surface. The symmetry of SBs has been perturbed before they flow to the free surface because of the existing of preceding indents. Thus, asymmetric SBs could be observed to the left of the indents. The SB characteristics shown in Fig. 7 indicate that the generation of new SBs, the reactivation and deflection of pre-existing SBs, and the intersection between new SBs and pre-existing SBs occur alternately during the nanoindentation test to accommodate the plastic deformation. That is, the main carrier of plastic deformation can alternate between the newly generated SBs and pre-existing SBs, depending on the occurrence of SB reactivation, stoppage or intersection.

In Fig. 7(a) and (b), the reactivation of pre-existing SBs is observed. This is thought to be one of the main factors affecting the subsequent plastic deformation of pre-deformed MGs [5,6,21,22,30]. However, any conclusion would not be very credible if the reactivation of pre-existing SBs were to be identified only by analyzing the SEM morphology. Hence, more credible evidence should be provided. As shown in Figs. 4 and 6, SBs are distributed in the pile-up regions around individual indents with visible steps, which result from the shear offset. Thus, a height difference exists for each SB (with the inner side of each SB being higher than the outer side). If one SB is reactivated to carry the subsequent plastic deformation, the height of the two sides of the SB might be reversed, i.e., the higher side becomes the lower side. Based on this concept, AFM was used to capture the topography of the interaction region where SB reactivation, as shown in Fig. 7(a), is thought to have occurred as a result of analyzing the SEM morphology.

Fig. 8(a) presents the SEM morphology where SB reactivation is thought to have occurred as indicated because its direction is consistent with that of the pre-existing SBs. Fig. 8(b) shows a top view of the

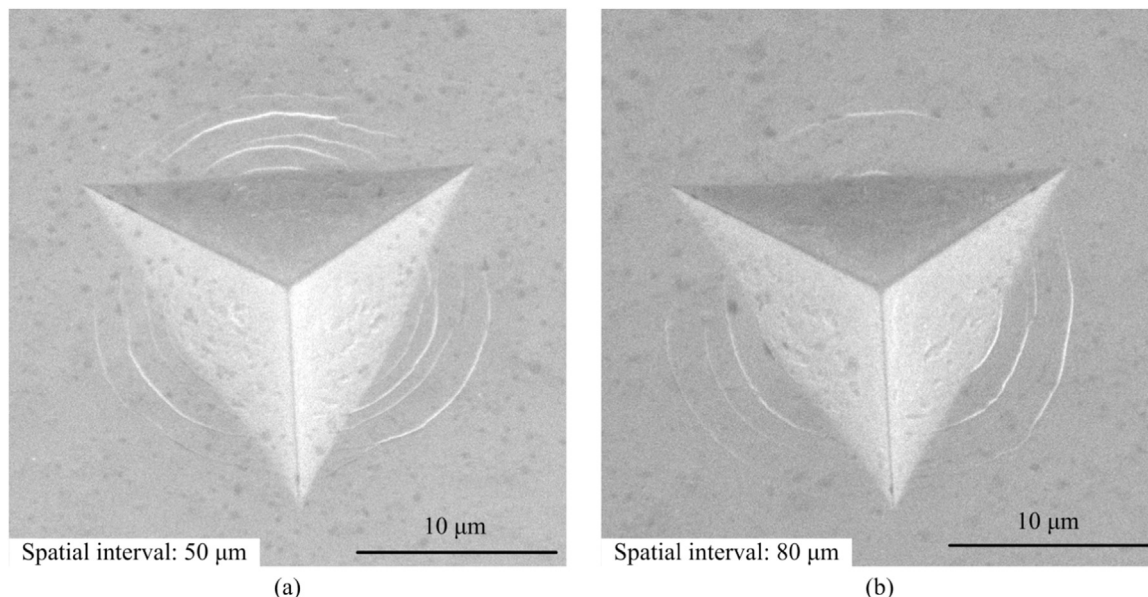


Fig. 6. Representative SEM morphologies of indents corresponding to intervals d of (a) 50 μm and (b) 80 μm .

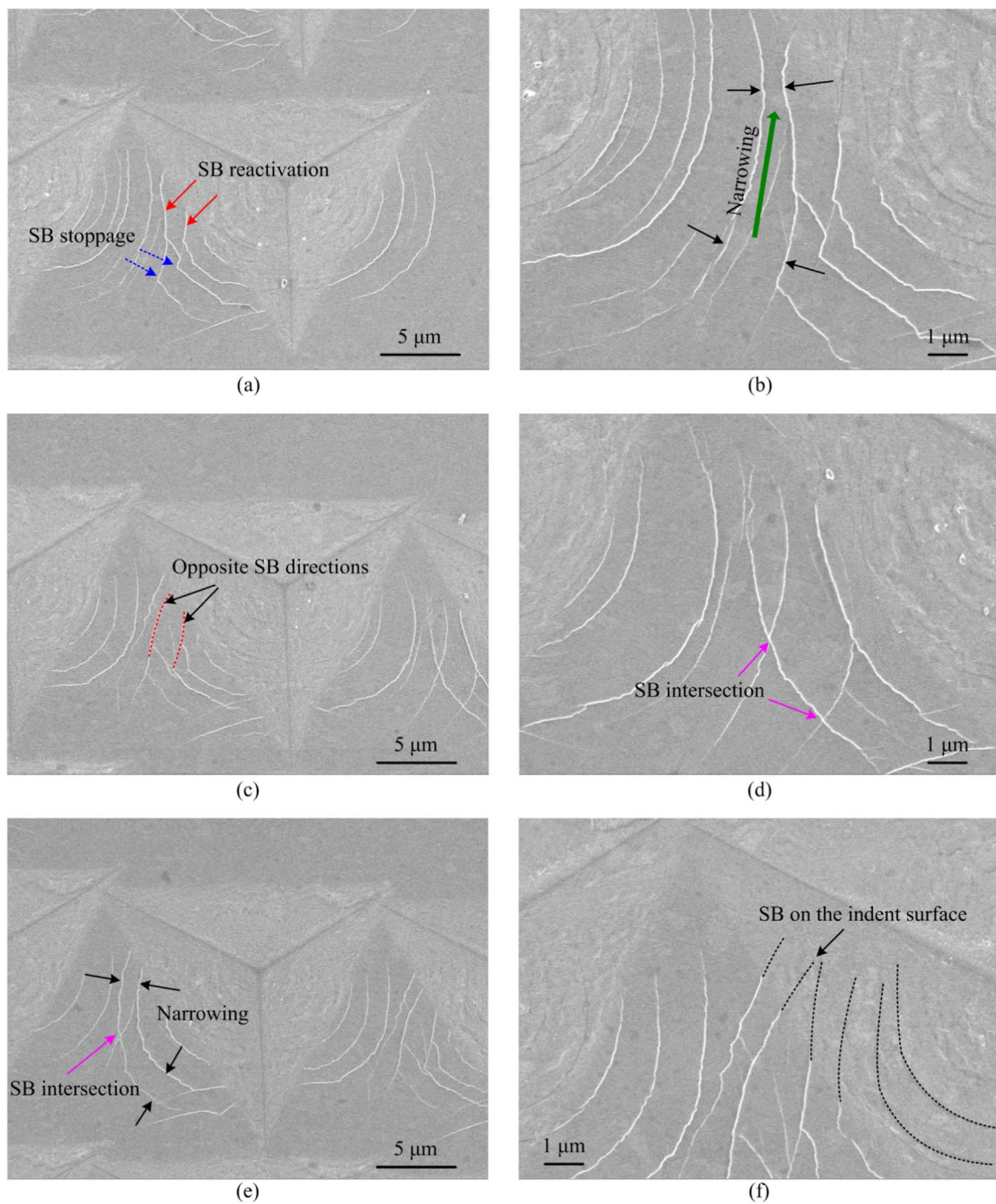


Fig. 7. Representative SEM morphologies of indents corresponding to interval d of 18 μm .

interaction region in Fig. 8(a). The profiles of lines with Nos. 1–4 in Fig. 8(b) are extracted as illustrated in Fig. 8(c)–(f), respectively, while the arrows in Fig. 8(b) denote the directions of measurement. Line 1 is in the region in which the SBs maintain an arc-like shape and steps with a remarkable difference in height are observed in its profile. Along the measuring direction, the height gradually increases, agreeing with the fact that the inner side of the SB is higher than the outer side. Lines 2 and 3 are measured across one SB at two different positions and this SB should belong to the left indent by analyzing its direction. Thus, in theory, the left side of this SB should be higher than the right side. While, in Fig. 8(d) and (e), it is interesting to note that the left side is lower than the right side, and the height of the two sides of the SB has been reversed, which confirms that reactivation of the pre-existing SB

has occurred during the subsequent nanoindentation test. Line 4 is measured in the region where SB intersection has occurred. In Fig. 8(f), the height sequentially decreases, increases, decreases, and then increases again, indicating that no height reversal occurs when SB intersection occurs, with the newly generated SB merely passing through a pre-existing SB. These height features can be further visualized in the 3D AFM topography. The AFM results further experimentally confirm the occurrence of SB reactivation and intersection in the interaction region during adjacent nanoindentation tests.

Fig. 9 shows representative SEM morphologies of the indents corresponding to an interval d of 15 μm . Compared with the SEM morphologies shown in Figs. 5 and 7 corresponding to intervals d of 20 and 18 μm , respectively, the interaction regions in Fig. 9 show very few

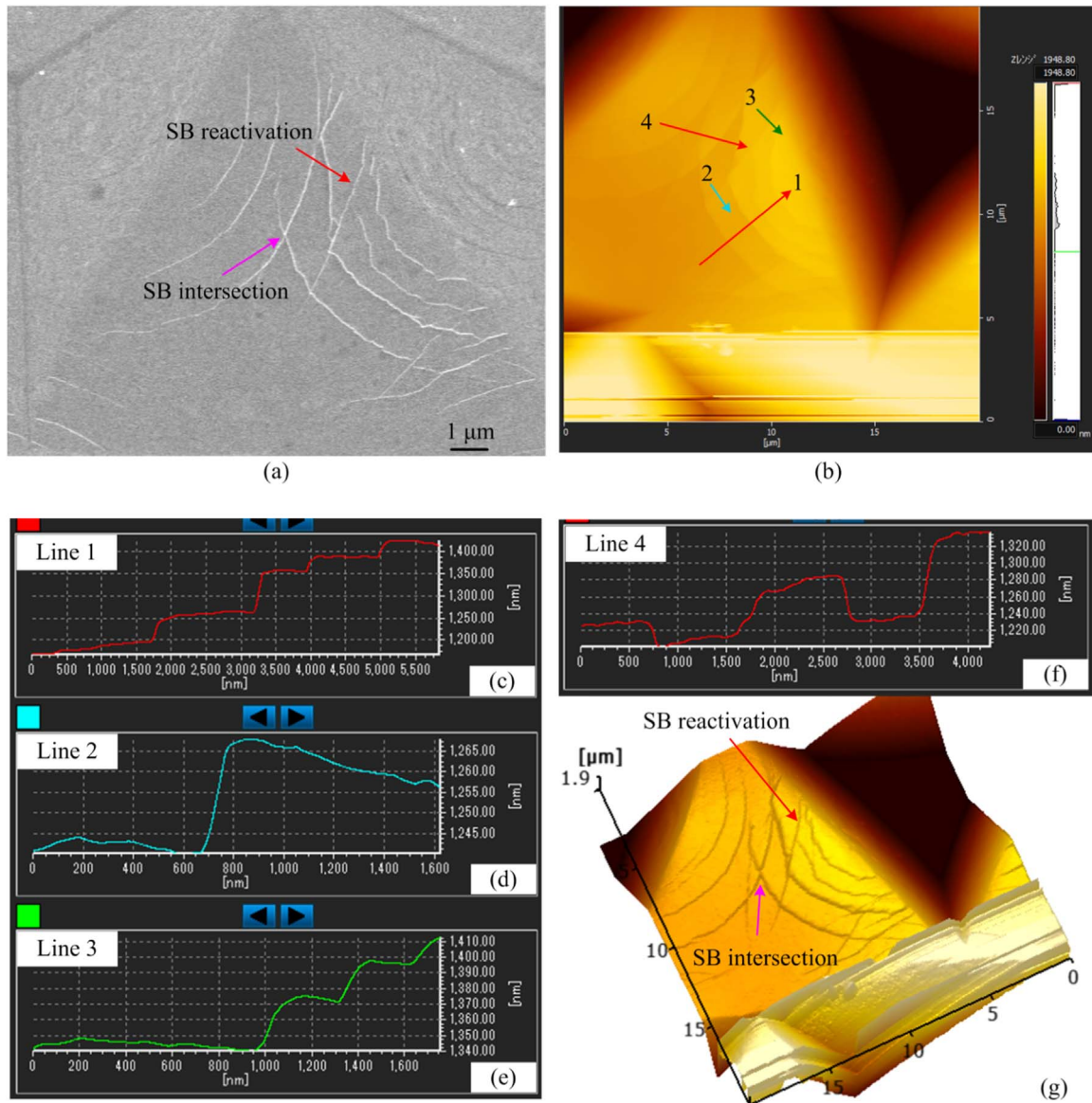


Fig. 8. (a) SEM morphology showing SB reactivation and intersection. (b) AFM image (top view) of interaction region in (a). (c)–(f) illustrating the profiles of the lines 1–4 in (b) respectively. (g) 3D AFM image showing topography of the interaction region.

newly generated SBs to the left of the indents although sometimes very weak new SBs can be observed as shown in Fig. 9(b). However, above and to the right of the indents, newly generated SBs are observed although portions of them have been cut off by subsequent indents because of the short interval of 15 μm. Furthermore, the inner SBs to the right of the indents are arc-shaped while the outer SBs exhibit multi-segments and SB deflection and mismatch can be observed, which may be a result of the complex stress in the interaction region. As shown in Fig. 9(a), when the interval decreases to 15 μm, both the left-hand and downside indents significantly affect the subsequent nanoindentation tests, while the effect of the downside indent is relatively weaker for intervals d of 18 and 20 μm. The difference in the SBs to the left, right and above the indents in Fig. 9 indicates that the plastic deformation to the left of the indent is mainly accommodated by the pre-existing SBs generated to the right of the left-hand indent and above the downside indent. Thus, nearly no new SBs are generated to the left of the indent. In addition, as shown in Fig. 9(d), the left half of the SBs above the indent is suppressed because a residual tension stress exists at the corner of the indent, agreeing well with the results of a previous report stated that residual tensile stress suppresses the generation of SBs [27].

3.2. Discussion on the various shear band characteristics

From the SEM morphologies shown in Figs. 5, 7, and 9, it is noted that various SB characteristics have been induced in the interaction regions corresponding to different spatial intervals. For an interval d of 20 μm, straight SBs and arc-shaped SBs coexist in the interaction region. With the decrease in the interval d to 18 μm, the number of straight SBs decreases and the reactivation of the pre-existing SBs as well as their interaction with the newly generated SBs, is observed. When the interval d further decreases to 15 μm, the generation of new SBs is significantly suppressed in the interaction region.

To rationalize the evolution of the SBs with a spatial interval d , both the pre-existing SBs and residual stress remaining around the preceding indents are considered. In Fig. 4, it can be observed that the indentation-affected region for an individual indent is about 24 μm. In Fig. 10, circles with a diameter of 24 μm are used to surround Nos. 1, 7, and 11 indents obtained with an interval d of 20 μm. For No. 1 indent, the indentation-affected region is obviously larger than the visible SB region. As the formation of the SBs is driven by the shear stress, the stress near the outer side of the indentation-affected region would be not

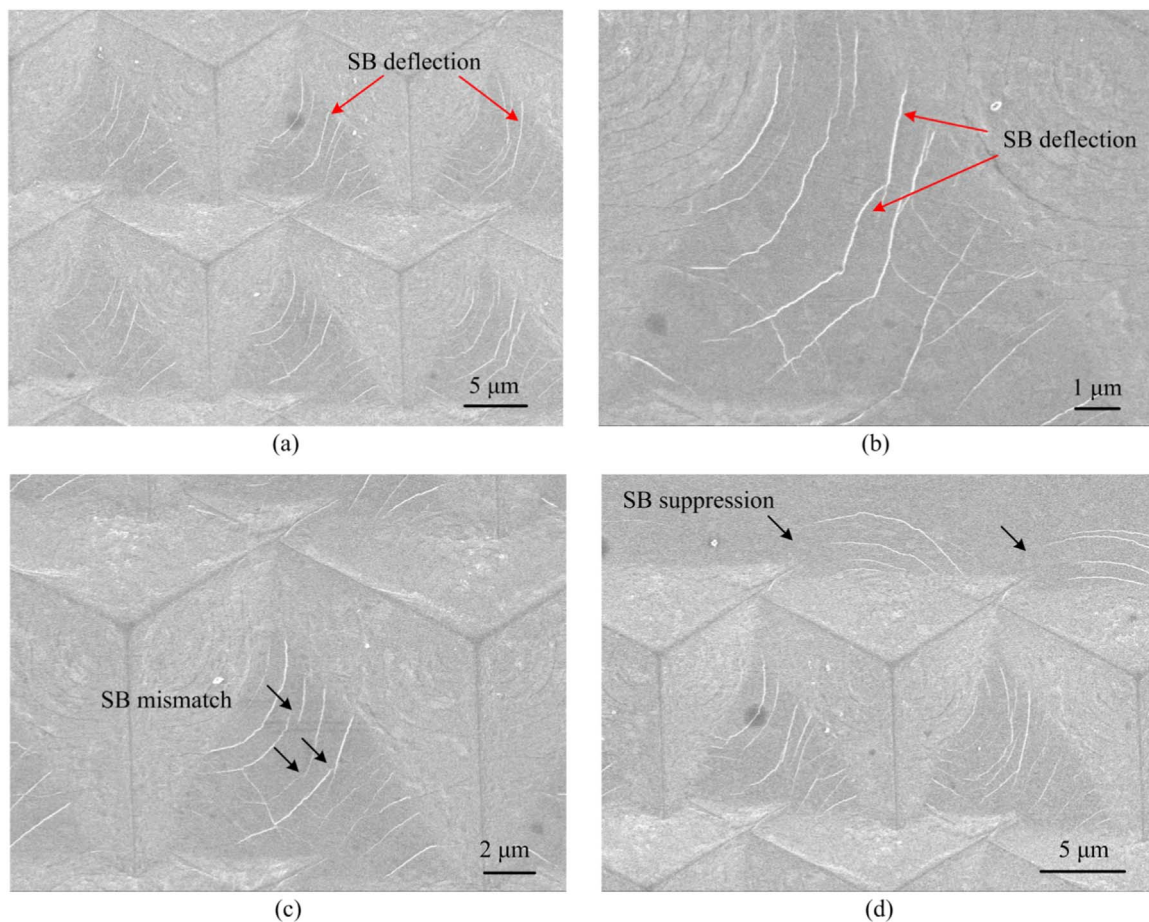


Fig. 9. Representative SEM morphologies of indents corresponding to an interval d of 15 μm .

sufficient to induce the formation of visible SBs and thus SBs can only be observed near the edges of the indent. For adjacent nanoindentation tests with an interval d of 20 μm (Nos. 7 and 11 indents, for example), the visible pre-existing SBs to the right of Nos. 7 indent is near the margin of the indentation-affected region of No. 11 indent, but they are rather far from the edge of No. 11 indent. Hence, the reactivation of these pre-existing SBs around No. 7 indent is difficult and new SBs have to be generated to accommodate the plastic deformation on the left side of No. 11 indent. In this case, the main carrier of the plastic deformation to the left of the indent is the newly generated SBs. As a portion of the

indentation-affected region of No. 11 indent overlaps with that of No. 7 indent, the direction of the newly generated SBs in this overlapped region is controlled not only by the stress from the No. 11 nanoindentation but also from the residual stress of No. 7 indent. Their resultant stress leads to the formation of straight SBs in the interaction region rather than arc-shaped SBs. On the other hand, because the lower-left portions of Nos. 7 and 11 indents are not in the overlapped regions, the corresponding SBs basically maintain their arc-shape.

As the interval d decreases to 18 μm , the overlap of the indentation-affected regions increases and the pre-existing SBs to the right of

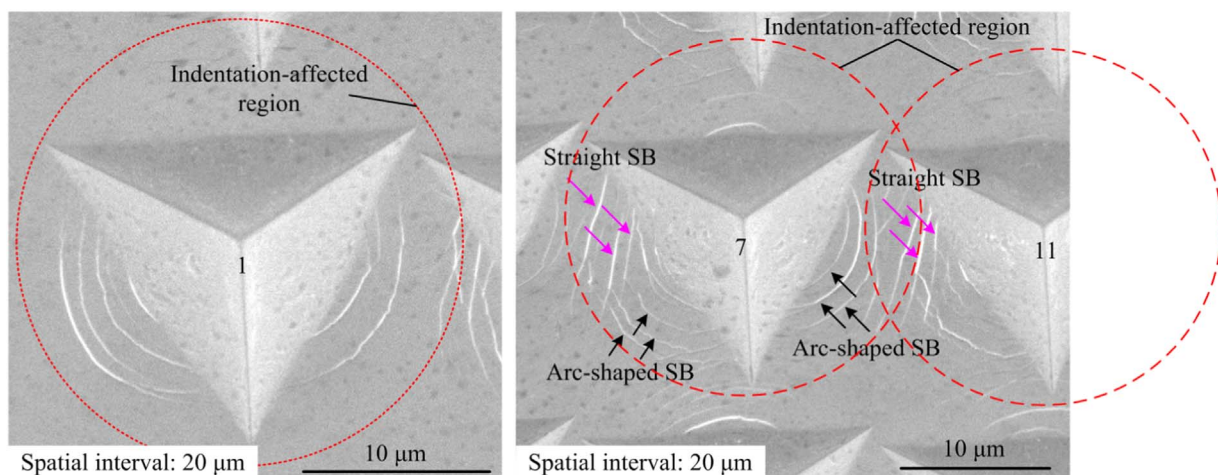


Fig. 10. Indentation-affected regions and SBs corresponding to an interval d of 20 μm .

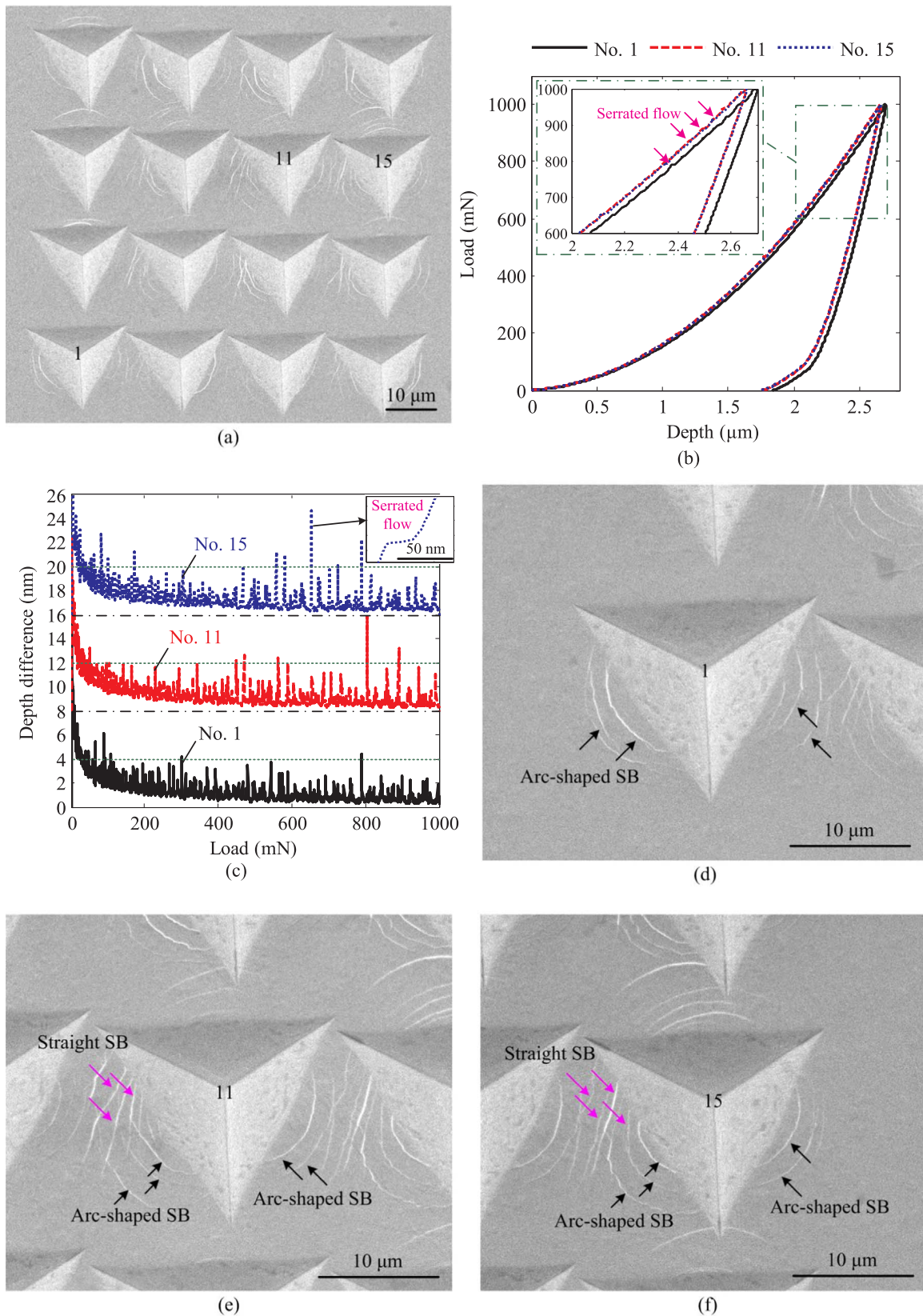


Fig. 11. (a) SEM morphology of indentation region corresponding to an interval d of 20 μm and a loading rate of 5 mN/s. (b) Load-depth (P - h) curves and (c) depth difference-load curves corresponding to Nos. 1, 11 and 15 indents. (d)–(f) show the enlarged morphologies of Nos. 1, 11, and 15 indents, respectively.

preceding indents become closer to the edge of the current indent. Therefore, some pre-existing SBs are reactivated and deflected by the stress generated by the current indent and they interact with the SBs that are newly generated in the lower-left portion of the indents. Thus, SB reactivation, deflection, stoppage, and intersection can be observed for an interval d of 18 μm . In this case, the main carrier of the plastic deformation to the left of the indent alternates between the newly generated SBs and pre-existing SBs.

When the interval d further decreases to 15 μm , the overlapped regions further increase between two adjacent indents, and the down-side indent also overlaps the current indent. As shown in Fig. 9, although portions of the pre-existing SBs are cut off by the current indent, the direction of the residual pre-existing SBs are close to the normal direction of the left edge of the indent. Thus, the plastic deformation is readily accommodated by these pre-existing SBs and very few SBs are newly generated to the left of the indent. In this case, the main carrier of the plastic deformation to the left of the indent is the pre-existing SBs, generated to the right of the left-hand indent and above the downside indent.

3.3. Serrated flow

It has been reported [21,31,32] that operations of SBs result in discontinuous depth changes in the load-depth (P - h) curve, i.e. appearance of serrated flows. As various SB behaviors have been observed as a result of adjacent nanoindentation, it is derived that serrated flows are also likely to change. Thus, by investigating the change in serrated flows, the SB interaction could be further confirmed. As the nanoindentation results mentioned above were obtained with a loading rate of 100 mN/s, the serrated flows should have been significantly suppressed because of this fast loading rate [32,33]. To effectively stimulate the serrated flows, a relatively slow loading rate of 5 mN/s was selected and one 4×4 nanoindentation array was formed with an interval d of 20 μm .

Fig. 11(a) shows the SEM morphology of the indentation region. Compared with the SBs shown in Fig. 5(a), obtained with a loading rate of 100 mN/s, the SBs shown in Fig. 11(a) do not exhibit any major differences as mentioned in Section 2.2. Furthermore, similar straight SBs are induced in the interaction regions. According to the SEM morphologies, two typical indents (Nos. 11 and 15) with intensive SBs in the interaction regions are selected for comparison with the No. 1 indent. Fig. 11(b) illustrates their P - h curves. It is noted that the P - h curves for Nos. 11 and 15 indents overlap each other well and their corresponding maximum indentation depths are slightly less than that for No. 1 indent. In consideration of the change in surface topography after preceding nanoindentation tests, the effects of preceding indents on the hardness of subsequent indents are not quantitatively discussed here. The inset in Fig. 11(b) shows a close-up view of the loading corresponding to a load range of 600–1000 mN. However, it is difficult to distinguish any difference in the serrated flows by observing only the P - h curve. To identify the difference in the serrated flows, the depth difference method [34] is used and the depth difference-load curves corresponding to Nos. 1, 11, and 15 indents are illustrated in Fig. 11(c). The curves for Nos. 11 and 15 indents are shifted by 8 and 16 nm, respectively along the vertical axis for clarity. Each peak in Fig. 11(c) denotes one serrated flow, with the higher peak indicating a larger burst depth during the serrated flow as shown in the example in the inset. Compared with the depth difference-load curve for No. 1 indent, more peaks with a height exceeding 4 nm are observed for Nos. 11 and 15 indents, indicating that the serrated flows have been promoted in their P - h curves.

To correlate the serrated flows with the SB characteristics, Fig. 11(d)–(f) show the residual indent morphologies of Nos. 1, 11, and 15 indents, respectively. There may be two main reasons for the promotion of the serrated flows for Nos. 11 and 15 indents. In Fig. 11(e) and (f), both straight and arc-shaped SBs are generated to the left of the

indents because of the complex stress in the interaction region, and the interaction between these two types of SBs, for example stoppage and intersection, could contribute to the promotion of the serrated flows. On the other hand, compared with the No. 1 nanoindentation test, the preceding indents increase the flow resistance of materials on its left and lower sides, and thus plastic flow is forced on the upper side as more SBs are observed on this side of Nos. 11 and 15 indents. The generation of new SBs should also promote the serrated flows. According to the characteristics of the SBs and serrated flows, it is concluded that plastic deformation during subsequent nanoindentation tests has been significantly affected by the preceding indents with SBs and residual stress.

4. Conclusions

Shear band (SB) interactions in Zr-based MGs were investigated by the adjacent nanoindentation method. Comparative experiments and analyses yielded the following conclusions.

- 1) The adjacent nanoindentation method was feasible to induce various SB behaviors by changing the spatial interval.
- 2) The reactivation of pre-existing SBs was experimentally confirmed by the appearance of height reversal at the two sides of the pre-existing SBs. Upon the reactivation of a pre-existing SB, the newly generated SBs could be stopped at the reactivated SBs, and the carrier of the plastic deformation could change from the newly generated SB to the reactivated SB. While, upon the occurrence of SB intersection, the newly generated SBs simply passed through the pre-existing SBs and the carrier of the plastic deformation remained as the newly generated SBs.
- 3) With a decrease in the interval from 20 to 18 μm , the main carrier of the plastic deformation in the interaction region changed from the newly generated SBs to an alternation between the newly generated SBs and pre-existing SBs. When the interval further decreased to 15 μm , the plastic deformation in the interaction region was readily accommodated by the pre-existing SBs, such that the generation of new SBs was considerably suppressed.
- 4) For a spatial interval of 20 μm , the preceding indents promoted serrated flows during subsequent nanoindentation tests, which may be a result of the SB interaction as well as the promoted generation of new SBs above the indent.

Acknowledgments

This study was partially supported by Grant-in-Aid for JSPS Fellows (Grant no. 26-04048).

References

- [1] Y.H. Liu, G. Wang, R.J. Wang, D.Q. Zhao, M.X. Pan, W.H. Wang, Super plastic bulk metallic glasses at room temperature, *Science* 315 (2007) 1385–1388.
- [2] J. Plummer, W.L. Johnson, Is metallic glass poised to come of age? *Nat. Mater.* 14 (2015) 553–555.
- [3] A.L. Greer, Y.Q. Cheng, E. Ma, Shear bands in metallic glasses, *Mater. Sci. Eng. R* 74 (2013) 71–132.
- [4] T.C. Hufnagel, C.A. Schuh, M.L. Falk, Deformation of metallic glasses: recent developments in theory, simulations, and experiments, *Acta Mater.* 109 (2016) 375–393.
- [5] Q.P. Cao, J.W. Liu, K.J. Yang, F. Xu, Z.Q. Yao, A. Minkow, H.J. Fecht, J. Ivanisenko, L.Y. Chen, X.D. Wang, S.X. Qu, J.Z. Jiang, Effect of pre-existing shear bands on the tensile mechanical properties of a bulk metallic glass, *Acta Mater.* 58 (2010) 1276–1292.
- [6] J. Kobata, T. Kimura, Y. Takigawa, T. Uesugi, H. Kimura, K. Higashi, Effect of pre-introduced shear bands direction on deformation behavior in Zr55Al10Ni5Cu30 bulk metallic glass, *Mater. Trans.* 50 (2009) 2355–2358.
- [7] Y. Zhang, W.H. Wang, A.L. Greer, Making metallic glasses plastic by control of residual stress, *Nat. Mater.* 5 (2006) 857–860.
- [8] C.C. Hays, C.P. Kim, W.L. Johnson, Microstructure controlled shear band pattern formation and enhanced plasticity of bulk metallic glasses containing in situ formed ductile phase dendrite dispersions, *Phys. Rev. Lett.* 84 (2000) 2901–2904.
- [9] M.L. Lee, Y. Li, C.A. Schuh, Effect of a controlled volume fraction of dendritic

- phases on tensile and compressive ductility in La-based metallic glass, *Acta Mater.* 52 (2004) 4121–4131.
- [10] X.F. Liu, Y. Chen, M.Q. Jiang, P.K. Liaw, L.H. Dai, Tuning plasticity of in-situ dendrite metallic glass composites via the dendrite-volume-fraction-dependent shear banding, *Mater. Sci. Eng. A – Struct.* 680 (2017) 121–129.
- [11] Y.J. Liu, H.W. Yao, T.W. Zhang, Z. Wang, Y.S. Wang, J.W. Qiao, H.J. Yang, Z.H. Wang, Designing ductile CuZr-based metallic glass matrix composites, *Mat. Sci. Eng. A – Struct.* 682 (2017) 542–549.
- [12] S. Xie, E.P. George, Hardness and shear band evolution in bulk metallic glasses after plastic deformation and annealing, *Acta Mater.* 56 (2008) 5202–5213.
- [13] B.G. Yoo, Y.J. Kim, J.H. Oh, U. Ramamurty, J.I. Jang, On the hardness of shear bands in amorphous alloys, *Scr. Mater.* 61 (2009) 951–954.
- [14] B. Shi, Y.L. Xu, C. Li, W.T. Jia, Z.Q. Li, J.G. Li, Evolution of free volume and shear band intersections and its effect on hardness of deformed Zr_{64.13}Cu_{15.75}Ni_{10.12}Al₁₀ bulk metallic glass, *J. Alloy. Compd.* 669 (2016) 167–176.
- [15] H. Bei, S. Xie, E.P. George, Softening caused by profuse shear banding in a bulk metallic glass, *Phys. Rev. Lett.* 96 (2006) 105503.
- [16] R. Maass, K. Samwer, W. Arnold, C.A. Volkert, A single shear band in a metallic glass: local core and wide soft zone, *Appl. Phys. Lett.* 105 (2014) 171902.
- [17] C.E. Packard, C.A. Schuh, Initiation of shear bands near a stress concentration in metallic glass, *Acta Mater.* 55 (2007) 5348–5358.
- [18] J.H. Perepezko, S.D. Imhoff, M.W. Chen, J.Q. Wang, S. Gonzalez, Nucleation of shear bands in amorphous alloys, *Proc. Natl. Acad. Sci. USA* 111 (2014) 3938–3942.
- [19] D. Klaumunzer, A. Lazarev, R. Maass, F.H.D. Torre, A. Vinogradov, J.F. Löffler, Probing shear-band initiation in metallic glasses, *Phys. Rev. Lett.* 107 (2011) 185502.
- [20] R. Maass, J.F. Löffler, Shear-band dynamics in metallic glasses, *Adv. Funct. Mater.* 25 (2015) 2353–2368.
- [21] H. Huang, J.L. Zhang, C.H. Shek, J.W. Yan, Effects of pre-compression deformation on nanoindentation response of Zr₆₅Cu₁₅Al₁₀Ni₁₀ bulk metallic glass, *J. Alloy. Compd.* 674 (2016) 223–228.
- [22] L. Wang, L. Wang, Y.F. Xue, H.F. Zhang, H.M. Fu, Nanoindentation response of laser shock peened Ti-based bulk metallic glass, *AIP Adv.* 5 (2015) 057156.
- [23] D.P. Wang, B.A. Sun, X.R. Niu, Y. Yang, W.H. Wang, C.T. Liu, Mutual interaction of shear bands in metallic glasses, *Intermetallics* 85 (2017) 48–53.
- [24] H. Huang, J.W. Yan, On the surface characteristics of a Zr-based bulk metallic glass processed by microelectrical discharge machining, *Appl. Surf. Sci.* 355 (2015) 1306–1315.
- [25] H. Huang, J.W. Yan, Microstructural changes of Zr-based metallic glass during microelectrical discharge machining and grinding by a sintered diamond tool, *J. Alloy. Compd.* 688 (2016) 14–21.
- [26] H. Huang, H. Zhao, Indenter geometry affecting indentation behaviors of the Zr-based bulk metallic glass, *Mater. Trans.* 55 (2014) 1400–1404.
- [27] F. Haag, D. Beitelshmidt, J. Eckert, K. Durst, Influences of residual stresses on the serrated flow in bulk metallic glass under elastostatic four-point bending – a nanoindentation and atomic force microscopy study, *Acta Mater.* 70 (2014) 188–197.
- [28] L. Wang, H. Bei, Y.F. Gao, Z.P. Lu, T.G. Nieh, Effect of residual stresses on the onset of yielding in a Zr-based metallic glass, *Acta Mater.* 59 (2011) 7627–7633.
- [29] P. Murali, U. Ramamurty, Embrittlement of a bulk metallic glass due to sub-T-g annealing, *Acta Mater.* 53 (2005) 1467–1478.
- [30] Y.F. Cao, X. Xie, J. Antonaglia, B. Winiarski, G. Wang, Y.C. Shin, P.J. Withers, K.A. Dahmen, P.K. Liaw, Laser shock peening on Zr-based bulk metallic glass and its effect on plasticity: experiment and modeling, *Sci. Rep.* 5 (2015) 10789.
- [31] C.A. Schuh, T.C. Hufnagel, U. Ramamurty, Overview no. 144 – mechanical behavior of amorphous alloys, *Acta Mater.* 55 (2007) 4067–4109.
- [32] C.A. Schuh, T.G. Nieh, A nanoindentation study of serrated flow in bulk metallic glasses, *Acta Mater.* 51 (2003) 87–99.
- [33] C.A. Schuh, T.G. Nieh, Y. Kawamura, Rate dependence of serrated flow during nanoindentation of a bulk metallic glass, *J. Mater. Res.* 17 (2002) 1651–1654.
- [34] H. Huang, H.W. Zhao, Z.Y. Zhang, Z.J. Yang, Z.C. Ma, Influences of sample preparation on nanoindentation behavior of a Zr-based bulk metallic glass, *Materials* 5 (2012) 1033–1039.